Refinement and homogenization of M_7C_3 carbide in hypereutectic Fe-Cr-C coating by Y_2O_3 and TiC

Sha Liu[a], Jin Zhang[b], Zhijie Wang[a], Zhijun Shi[a], Yefei Zhou[a,b], Xuejun Ren[c], Qingxiang Yang[a,□]
a State Key Laboratory of Metastable Materials Science & Technology, Yanshan University, Qinhuangdao 066004, PR China
b College of Mechanical Engineering, Yanshan University, Qinhuangdao 066004, PR China
c School of Engineering, Liverpool John Moores University, Liverpool L3 3AF, UK
key words: Hypereutectic Fe-Cr-C coating,7C3 carbide, Nano- Y_2O_3, TiC, Heterogeneous nucleation, Refinement

Abstract

The microstructures of the hypereutectic Fe-Cr-C, Fe-Cr-C-Ti and Fe-Cr-C-Ti- Y_2O_3coatings were observed by OM. The phase structures were characterized by XRD and XPS. The elemental distributions were analyzed by EDS. The interface relationship between TiC and nano- Y_2O_3 were observed by TEM and analyzed by lattice misfit theory. From the metallographic observations, the primary M_7C_3 carbide can be refined by Ti additive, while it is inhomogeneously distributed. However, the primary M_7C_3 carbide can also be refined further by adding Ti additive and nano- Y_2O_3 simultaneously, and it is homogeneously distributed. From the phase constituent analysis, TiC is formed by Ti additive, while TiC and Y_2O_3 are found by adding Ti additive and nano- Y_2O_3 simultaneously. From the elemental distribution mappings and TEM images, TiC nucleates upon nano- Y_2O_3 with orientation relationship {001} Y_2O_3//{001}TiC in the hypereutectic Fe-Cr-C-Ti-Y2O3 coating. By misfit compu- tation, the lattice misfit between Y_2O_3 (001) plane and TiC (001) plane is 7.3%, which suggests that Y_2O_3 can act as the heterogeneous nucleus of TiC so that TiC particles are increased and dispersedly distributed. These numerous dispersed TiC particles can further act as the heterogeneous nucleus of the primary M_7C_3 carbide, which play a role in refining primary M_7C_3 carbide and promoting its homogenization.

1. Introduction

With excellent wear-resistance, hypereutectic Fe-Cr-C coating has aroused wide concern in the arc surfacing additive manufacturing field [1,2]. However, as the main strengthening phase, the primary M_7C_3 carbide is easy to desquamate from the substrate due to its coarse size [3,4], which restricts the application of hypereutectic Fe-Cr-C coating in 3D-printing field.

Currently, ceramic phases such as TiC, which can play a role in refining the microstructure as heterogeneous nucleus, have been widely applied as reinforced particles in coatings to enhance the wear-re- sistance [5,6]. G. S. P. Kumar et al. [7] studied the microstructure of in situ fabricated AA6061-TiC composite and found that grains are refined due to the dispersed TiC particles. S.M. Hong et al. [8] added nano- sized TiC particles into SA-106B carbon steel and found that the grain size was reduced considerably with an increase in the TiC content.

In recent years, rare earth oxides have attracted great attention of researchers for their modifying, refining and purifying effects [9–11]. Many investigations show that rare earth oxides doped composites possess finer structures. J.F. Li et al. [12] investigated the effect of La_2O_3 additions on grain size of La_2O_3/W composite, and the results demonstrate that its mean grain size is decreased by La_2O_3. H.X. Qu et al. [13] studied the effect of CeO_2 on the microstructure of WC- 40%Al_2O_3 composite, which reveals that CeO_2 promotes its micro- structural refinement.

Our research group have added Ti/Nb additives into hypereutectic Fe-Cr-C coating by arc surfacing welding method and found that the previously precipitated MC (namely TiC and NbC) particles can act as the heterogeneous nucleus of the primary M_7C_3 carbide and thereby refines it [14,15]. We have also doped rare earth oxides such as La_2O_3, Y_2O_3 and CeO_2 into hypereutectic Fe-Cr-C coating, and found that they can also act as the heterogeneous nucleus and refine the primary M_7C_3 carbide [16–18]. However, if Ti/Nb additives and rare earth oxides are added into hypereutectic Fe-Cr-C coating simultaneously, whether the microstructure of the hypereutectic Fe-Cr-C coating can be further re- fined or not? At present, no researches have been reported.

In this paper, hypereutectic Fe-Cr-C, Fe-Cr-C-TiC and Fe-Cr-C-TiC- Y_2O_3 coatings were prepared by arc surfacing welding method. Based on the work that Ti additive was added, nano- Y_2O_3 particles were further added in order to investigate the refining effect of TiC and Y_2O_3 on the primary M_7C_3 carbide in hypereutectic Fe-Cr-C-TiC- Y_2O_3 coating, which can provide the foundation for the wide application of hypereutectic Fe-Cr-C coating in 3D-printing field.

Table 1
Parameters of welding process.

Wire diameter (mm)	Welding voltage (V)	Welding current (A)	Welding speed ($mm \cdot min^{-1}$.)
3.2	24–26	200–224	300

2. Experimental Methods

Three kinds of flux-cored wires were prepared by the following procedures. The mineral powders were mixed by using a three dimen- sional vibratory mill of 1400 r/min for 2 h. The H08A steel strip took "U" shape after multiple rolling. Then the fully mechanical-mixed powders were synchronously delivered to the U-shaped groove and the H08A steel strip passed through multiple forming-rollers step-by-step. Finally the O-shaped flux-cored wire was produced. In order to in- vestigate the effect of TiC, ferro-titanium powder ($d \approx 200$ μm) was added. In order to investigate the effect of TiC and Y_2O_3, ferro-titanium powder and nano- Y_2O_3 powder ($d \approx 200$ nm) were added simultaneously. The flux-cored wires were cladded on SS41 substrate by ZXG3–300-1 DC welder machine, by which hypereutectic Fe-Cr-C coating (wt%:3.5C + 26.7Cr + 1.0Si + 1.4Mn + 0.1 V + 0.1Ni + 0.5Al + Bal. Fe), hypereutectic Fe-Cr-C-Ti coating (adding 0.5 wt %Ti on the basis of hypereutectic Fe-Cr-C coating) and hypereutectic Fe-Cr-C-Ti- Y_2O_3 coating (adding trace amount of nano- Y_2O_3 on the basis of hypereutectic Fe-Cr-C-Ti coating) were prepared. The welding parameters are listed in Table.1.

Samples were polished and etched with 35%FeCl3 + 6% HNO3 + 2%HCl + 57%C2H5OH solution. And then microstructures were observed by Axiovert 200 MAT optical microscope (OM). The size of the primary M_7C_3 carbides were analyzed by Image-pro Plus 5.1.0 software. On account that the primary M_7C_3 carbide is irregular polygon, area statistics were used for size characterization for con- venience. The coatings were detected by D/max-2500/PC X-ray diffractometer (XRD). The surface composition of the hypereutectic Fe-Cr- C-Ti- Y_2O_3 coating was measured by Thermo VG Multilab2000 X-ray photo-emission spectroscopy (XPS). The elemental distributions of the coatings were measured by EMAX energy dispersive spectrometer. In addition, foil specimen cut from hypereutectic Fe-Cr-C-Ti- Y_2O_3 coating was mechanical polished and thinned by Gatan precision ion polishing system (PIPS). Then the foil specimen was observed by JEM-2010 transmission electron microscopy (TEM). The dispersion of TiC in Fe-Cr-C-Ti and Fe-Cr-C-Ti- Y_2O_3 coatings were observed by Hitachi S3400 N back-scattering scanning electron microscope (BSEM).

3. Results and Discussion

3.1. Size and Distribution of Primary M_7C_3 Carbide

Fig. 1 shows the metallographic images of the coatings, in which the white irregular polygons are the primary M_7C_3 carbides. The mean sizes of the primary M_7C_3 carbides in hypereutectic Fe-Cr-C, Fe-Cr-C-Ti and Fe-Cr-C-Ti-Y_2O_3coatings are 434.7 μm2, 168.8 μm2 and 94.2 μm2 re- spectively. From Fig. 1a and Fig. 1b, it is demonstrated that the primary M7C3 carbide can be refined by Ti additive, which is in consistence with previous researches [14,19]. The refinement is ascribed to the hetero- geneous nucleus role of TiC to primary M_7C_3 carbide. From Fig. 1b and Fig. 1c, the size of the primary M_7C_3 carbides becomes even smaller by nano- Y_2O_3, which means that adding Ti additive and nano- Y_2O_3into hypereutectic Fe-Cr-C coating simultaneously can further refine the primary M_7C_3 carbides. It also can be found from Fig. 1 that adding Ti and nano- Y_2O_3simultaneously can promote the uniform distribution of the primary M_7C_3 carbides.

Fig. 2 shows the size statistics of the primary M_7C_3 carbides in the coatings, in which each point represents a primary M_7C_3 carbide. It is found that the size span of the primary M_7C_3 carbides in hypereutectic Fe-Cr-C coating is the maximum, where the majority carbides are smaller than 1000 μm2, while the minority carbides are larger than 1000 μm2 and even several carbides reach 3000 μm2. Relatively, the majority carbides in hypereutectic Fe-Cr-C-Ti coating are smaller than 500 μm2, and only few are in the range of 500 μm2–1000 μm2. While, the size span of the primary M_7C_3 carbides in hypereutectic Fe-Cr-C-Ti- Y_2O_3 coating is quite small. The size statistics fluctuate near the mean size and only individual carbides reach 300–400 μm2. Fig. 2 illustrates that the dimension uniformity of the

primary M7C3 carbides can be improved by adding Ti and nano- Y_2O_3 simultaneously.

3.2. Phase Constituent Analysis

Fig.3 displays the XRD patterns of the coatings. It can be seen that the hypereutectic Fe-Cr-C coating mainly contains M_7C_3 carbide, γ-Fe (austenite). While the hypereutectic Fe-Cr-C-Ti and Fe-Cr-C-Ti- Y_2O_3 coatings also contain TiC besides of these two phases. However, Y_2O_3 is not detected in hypereutectic Fe-Cr-C-Ti- Y_2O_3 coating, which may be due to the trace amount of nano- Y_2O_3.
Fig. 4a shows the XPS spectra of the hypereutectic Fe-Cr-C-Ti- Y_2O_3 coating, which is calibrated with respect to the peak of C element. Y-3d peaks are found in the range of 150 eV–170 eV. Fig. 4b shows the XPS spectra of the Y-3d region. Two distinct peaks at 156.5 eV and 161.1 eV can be assigned to 3d5/2 and 3d3/2 of Y3+ respectively, which proves the existence of Y_2O_3 in hypereutectic Fe-Cr-C-Ti- Y_2O_3 coating.

3.3. Heterogeneous Nucleus Analysis

Fig. 5 shows the elemental distribution mappings of the hyper- eutectic Fe-Cr-C-Ti- Y_2O_3 coating. Based on the fact that the primary M_7C_3 carbide is rich in Cr, the green polygons in Fig. 5a are the primary M_7C_3 carbides. There is a Cr depletion region on the edge of the primary M_7C_3 carbide, which is marked by a circle. According to the Ti ele- mental distribution mapping in Fig. 5b, this region is rich in Ti. By further element analysis, the main elements in this region are Ti and C, which means that the Ti enriched and Cr depleted region is TiC particle, which is in agreement with the literature [14], namely TiC particle exists inside or on the edge of the primary M_7C_3 carbide. According to the Y elemental distribution mapping in Fig. 5c, there is obvious Y accumulation in the center of TiC.

Fig. 6a shows the bright field TEM image of a TiC particle, from which TiC is bloom shape. By extracting the selected area diffraction patterns (SADPs) of the “stamen” and “petal”, the corresponding dark field TEM images are displayed in Fig. 6b and Fig. 6c respectively. Accordingly, the “stamen” region is Y_2O_3 with diameter of 200 nm, which is the same size as the nano- Y_2O_3 particles added into the hy- pereutectic Fe-Cr-C-Ti- Y_2O_3 coating. Therefore, it further proves the existence of Y_2O_3 in the hypereutectic Fe-Cr-C-Ti- Y_2O_3 coating. The “petal” region consists of several TiC particles. Based on the phenomena in Fig. 6, it can be known that TiC nucleates upon nano- Y_2O_3.

B.L. Bramfitt [20] put forward the two-dimensional lattice misfit theory by a large amount of tests and computations, which is widely used in evaluating the validity of heterogeneous nucleation. Its math ematical model is as follow:

$$\delta_{(hkl)_n}^{(hkl)_s} = \sum_{i=1}^{3} [(|d_{[uvw]_s}{}^i \cos\theta - d_{[uvw]_n}{}^i|/d_{[uvw]_n}{}^i)/3] \times 100\%$$

where δ(hkl) (hkl)s is the lattice misfit, corner marks s and n represent substrate phase and nucleated phase respectively, (hkl) is a low-index plane, [uvw] is a low-index direction on (hkl), d[uvw] is the interatomic spacing along [uvw], θ is the angle between [uvw]s and [uvw]n.

According to the theory, δ(hkl) (hkl)s < 6% means the heterogeneous nucleus effect of the substrate phase on the nucleated phase is of high validity, while δ(hkl) (hkl)s =6% – 12% means medium validity and δ(hkl) (hkl)s > 12% means unavailability. TiC is NaCl-type structure with lattice parameter a = 4.33 Å [21], whose crystal structure is schematically shown in Fig.7a. Y_2O_3 is CaF2-type structure with disordered oxygen vacancy, whose lattice parameter is a = 5.63 Å [22] and the crystal structure is schematically shown in Fig.7b. By indexing the SADPs in Fig. 6b and Fig. 6c, the orientation relationship between Y_2O_3 and TiC is {001} Y_2O_3//{001}TiC and it is schematically displayed in Fig.7c. The atomic sites at the {001} Y_2O_3//{001}TiC interface is also schematically displayed in Fig.7d. The lattice misfit between Y_2O_3.
(1) plane and TiC (001) plane is 8.74%, which suggests that Y_2O_3can act as the heterogeneous nucleus of TiC. As a result, the amount of TiC can be increased and its size can be refined. It can be validated by the back-scattering micrographs of the hypereutectic Fe-Cr-C-Ti and Fe-Cr- C-Ti- Y_2O_3 coatings in Fig. 8, in which the darkest particles are TiC. It can be easily seen that the amount of TiC is increased and its diameter is reduced from about five microns to two microns. Previous researches have proved that M_7C_3 (0001)/TiC(111) interface is theoretically stable, and the preferentially precipitated TiC can refine the primary M_7C_3 carbide by acting as heterogeneous nucleus [14,19]. The amount in- crease of TiC particles will undoubtedly increase the heterogeneous nucleus of the primary M_7C_3 carbide, so that the refinement of the primary M_7C_3 carbide will be further enhanced. Before fabricating the coatings, the welding material powders are fully uniformly mixed. So the nano- Y_2O_3 particles are dispersedly distributed, which promotes the uniform distribution of TiC and contributes to the homogenization of the primary M_7C_3 carbides in a roundabout way. Therefore, nano- Y_2O_3 in the hypereutectic Fe-Cr-C-Ti- Y_2O_3 coating can accelerate the re- finement and homogenization of the primary M_7C_3 carbide. As a con- sequence, the comprehensive

performance of the hypereutectic Fe-Cr-C coating will be enhanced and the application of the hypereutectic Fe- Cr-C coating in 3D–printing field will be enlarged.

4. Conclusions

By adding Ti additive into hypereutectic Fe-Cr-C coating, the pri- mary M_7C_3 carbide can be refined, while it is inhomogeneously distributed. On this basis, by adding Ti additive and nano- Y_2O_3 si- multaneously, the further refined and homogenized primary M_7C_3 carbide can be obtained.

- The refinement and homogenization effect of nano- Y_2O_3 and TiC on the primary M_7C_3 carbide can be described as: i) TiC nucleates upon nano- Y_2O_3, which results in the amount increase and dispersed distribution of TiC particles. ii) The numerous dispersed TiC particles further act as the heterogeneous nucleus of the primary M_7C_3 carbide and promote its refinement and homogenization.

Acknowledgements

The authors would like to express their gratitude for projects sup- ported by the National Natural Science Foundation of China (No. 51471148), the Hebei province Basic Research Foundation of China (No. 16961008D) and the Innovation Fund for Graduate Students of Hebei Province (No. CXZZBS2017046).

Compliance with Ethical Standards

Conflict of interest: the authors declare that they have no conflict of interest.

References

[1] A. Zikin, I. Hussainova, C. Katsich, Advanced chromium carbide-based hardfacings, Surf. Coat. Technol. 206 (2012) 4270–4278.
[2] D.S. Liu, R.P. Liu, Y.H. Wei, Comparative behaviour of cobalt and iron base hard- facing alloys, Surf. Eng. 28 (2012) 338–344.
[3] X.W. Qi, Z.N. Jia, Q.X. Yang, Y.L. Yang, Eff ects of vanadium additive on structure property and tribological performance of high chromium cast iron hardfacing metal, Surf. Coat. Technol. 205 (2011) 5510–5514.
[4] X.H. Zhi, J.D. Xing, Y.M. Gao, H.G. Fu, J.Y. Peng, B. Xiao, Eff ect of heat treatment on microstructure and mechanical properties of a Ti-bearing hypereutectic high chromium white cast iron, Mater. Sci. Eng. A 487 (2008) 171–179.
[5] A. Farid, S.J. Guo, F. Cui, P.Z. Feng, T. Lin, TiB_2 and TiC stainless steel matrix composites, Mater. Lett. 61 (2007) 189–191.
[6] J.J. Liu, Z.D. Liu, An experimental study on synthesizing TiC-TiB_2-Ni composite coating using electro-thermal explosion ultra-high speed spraying method, Mater. Lett. 64 (2010) 684–687.
[7] G.S.P. Kumar, P.G. Koppad, R. Keshavamurthy, M. Alipour, Microstructure and mechanical behaviour of in situ fabricated AA6061-TiC metal matrix composites, Arch. Civ. Mech. Eng. 17 (2017) 535–544.
[8] S.M. Hong, E.K. Park, J.J. Park, M.K. Lee, J.G. Lee, Eff ect of nano-sized TiC particle addition on microstructure and mechanical properties of SA-106B carbon steel, Mater. Sci. Eng. A 643 (2015) 37–46.
[9] F. Han, Y. Bai, L.J. Qiao, D. Guo, A systematic modification of the large electro- caloric eff ect within a broad temperature range in rare-earth doped $BaTiO_3$ cera- mics, J. Mater. Chem. C 4 (2016) 1842–1849.
[10] D.R. Ou, T. Mori, F. Ye, T. Kobayashi, J. Zou, G. Auchterlonie, J. Drennan, Oxygen vacancy ordering in heavily rare-earth-doped ceria, Appl. Phys. Lett. 89 (2006) 171911.
[11] X. Zhang, Y. Sui, X. Wang, Y. Wang, Z. Wang, Eff ect of Eu substitution on the crystal structure and multiferroic properties of $BiFeO_3$, J. Alloys Compd. 507 (2010) 157–161.
[12] J.F. Li, J.G. Cheng, B.Z. Wei, M.L. Zhang, L.M. Luo, Y.C. Wu, Microstructure and properties of La_2O_3 doped W composites prepared by a wet chemical process, Int. J. Refract. Met. Hard Mater. 66 (2017) 226–233.
[13] H.X. Qu, S.G. Zhu, P. Di, C.X. Ouyang, Q. Li, Microstructure and mechanical properties of WC-40vol%Al_2O_3 composites hot pressed with MgO and CeO_2 ad- ditives, Ceram. Int. 39 (2013) 1931–1942.
[14] S. Liu, Y.F. Zhou, X.L. Xing, J.B. Wang, Q.X. Yang, Refining eff ect of TiC on primary M_7C_3 in hypereutectic Fe-Cr-C harden-surface welding coating: experimental re- search and first-principles calculation, J. Alloys Compd. 691 (2017) 239–249.
[15] S. Liu, Z.J. Wang, Z.J. Shi, Y.F. Zhou, Q.X. Yang, Experiments and calculations on refining mechanism of NbC on primary M_7C_3 carbide in hypereutectic Fe-Cr-C alloy, J. Alloys Compd. 713 (2017) 108–118.
[16] D. Li, Y.L. Yang, L.G. Liu, J.Z. Zhang, Q.X. Yang, Eff ects of RE oxide on the mi- crostructure of hardfacing metal of the large gear, Mater. Sci. Eng. A 509 (2009) 94–97.
[17] J. Yang, J.J. Tian, F.F. Hao, T. Dan, X.J. Ren, Y.L. Yang, Q.X. Yang, Microstructure and wear resistance of the hypereutectic Fe-Cr-C alloy hardfacing metals with dif- ferent La_2O_3 additives, Appl. Surf. Sci. 289 (2014) 437–444.
[18] J. Yang, X.R. Hou, P. Zhang, Y.F. Zhou, Y.L. Yang, X.J. Ren, Q.X. Yang, Mechanical properties of the hypereutectoid Fe-Cr-C hardfacing coatings with diff erent nano- Y_2O_3 additives and the mechanism analysis, Mater. Sci. Eng. A 655 (2016) 346–354.
[19] X.J. Wu, J.D. Xing, H.G. Fu, X.H. Zhi, Eff ect of titanium on the morphology of primary M_7C_3 carbides in hypereutectic high chromium white iron, Mater. Sci. Eng. A 457 (2007) 180–185.
[20] B.L. Bramfitt, Planar lattice disregistry theory and its application on heterogistry nuclei of metal, Metall. Trans. A. 1 (1970) 1987–1995.
[21] X.Z. Wu, T. Sun, R. Wang, L.L. Liu, Q. Liu, Energy investigations on the adhesive properties of al/TiC interfaces: first-principles study, Physica B 449 (2014) 269–273.
[22] J.L. De Mol Van Otterloo, J.Th.M. De Hosson, Microstructural features and me- chanical properties of a cobalt-based laser

coating, Acta Mater. 45 (1997) 1225–1236.

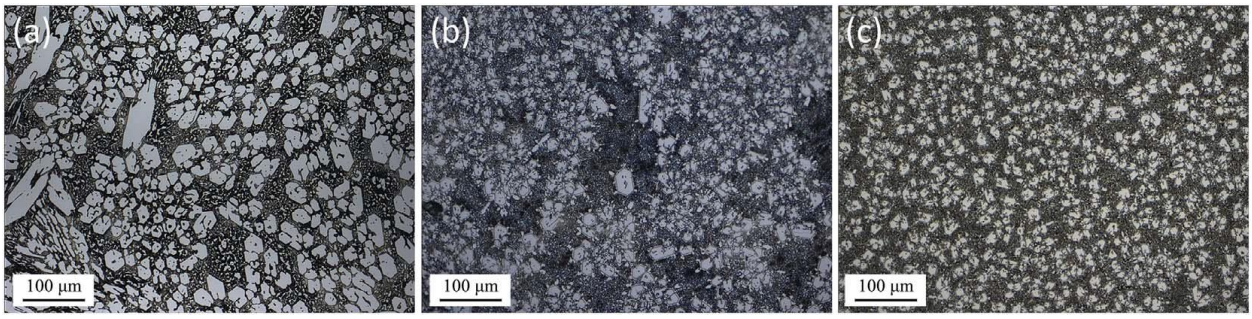

Fig. 1. Microstructures of (a) hypereutectic Fe-Cr-C coating, (b) hypereutectic Fe-Cr-C-Ti coating and (c) hypereutectic Fe-Cr-C-Ti- Y_2O_3 coating.

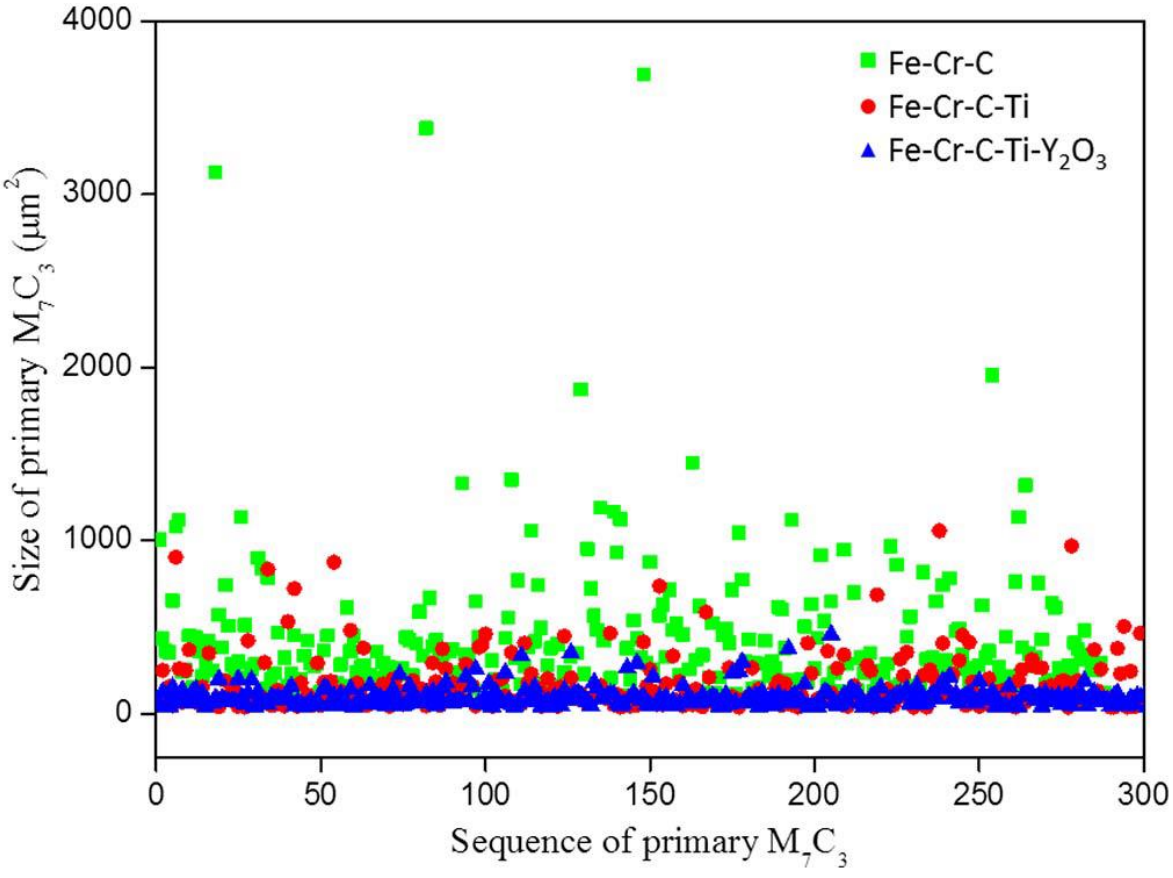

Fig. 2. Primary carbide size statistics of hypereutectic Fe-Cr-C coating, hypereutectic Fe- Cr-C-Ti coating and hypereutectic Fe-Cr-C-Ti- Y_2O_3 coating.

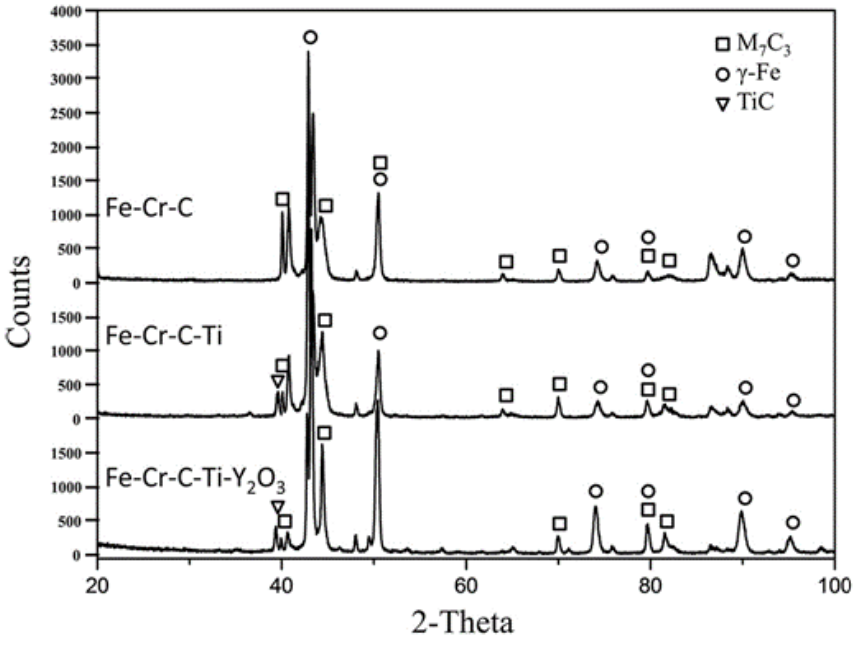

Fig. 3. XRD patterns of hypereutectic Fe-Cr-C coating, hypereutectic Fe-Cr-C-Ti coating and hypereutectic Fe-Cr-C-Ti-Y_2O_3 coating.

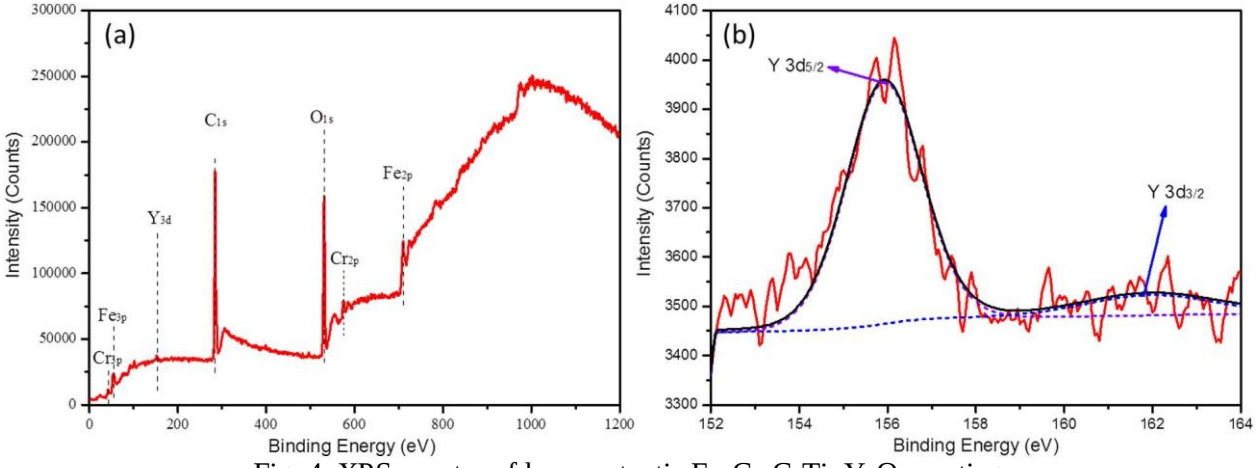

Fig. 4. XPS spectra of hypereutectic Fe-Cr-C-Ti- Y_2O_3 coating.

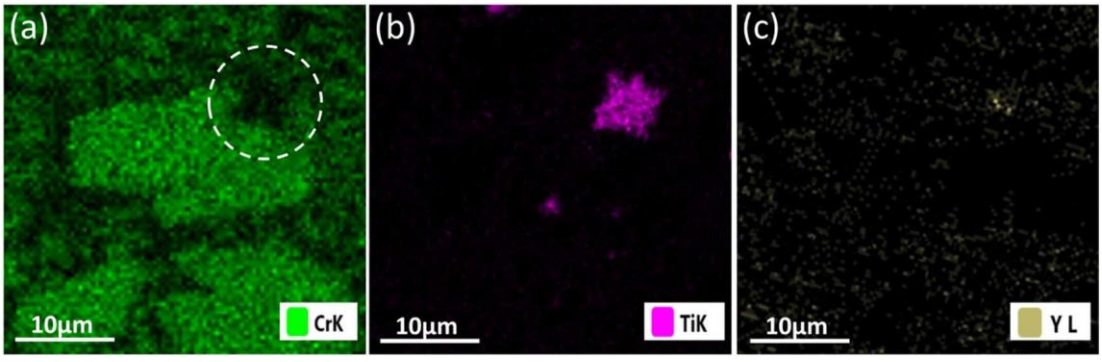

Fig. 5. Elemental distribution mappings of hypereutectic Fe-Cr-C-Ti- Y_2O_3 coating.

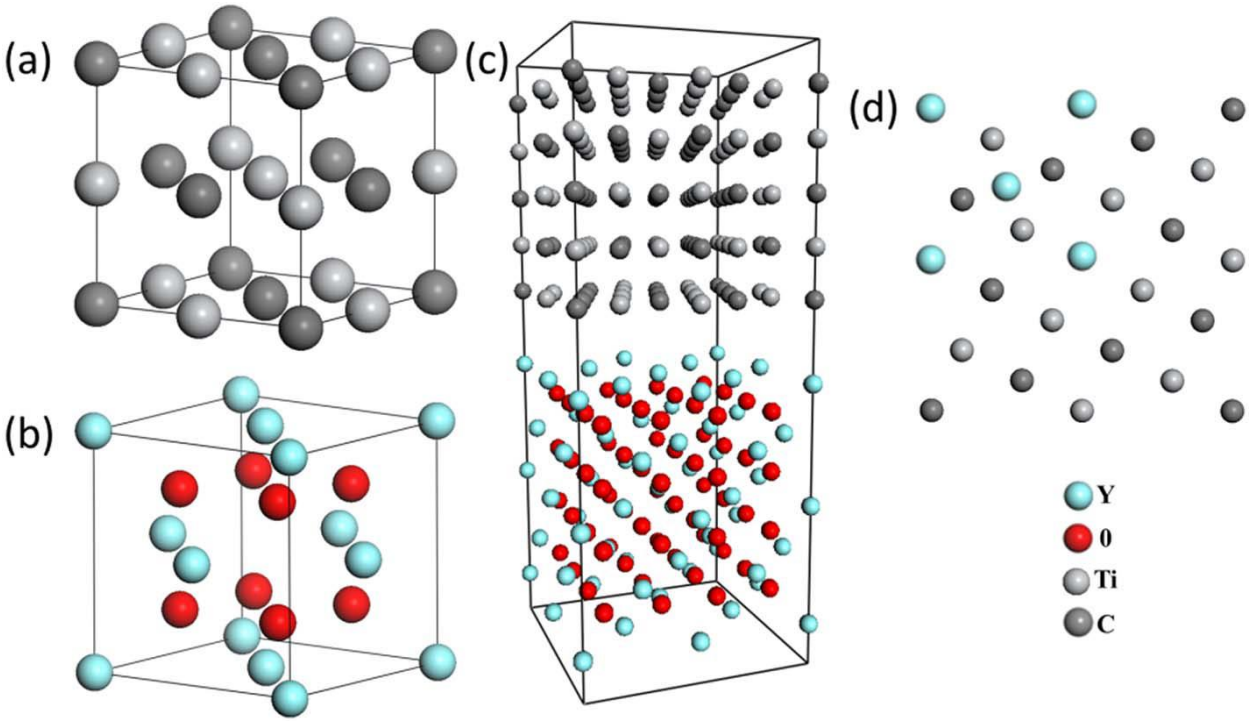

Fig. 7. Schematic illustrations of (a) TiC and (b) Y_2O_3 crystals; (c) {001}Y2O3//{001}TiC relationship; (d) atomic sites at Y_2O_3/TiC interface

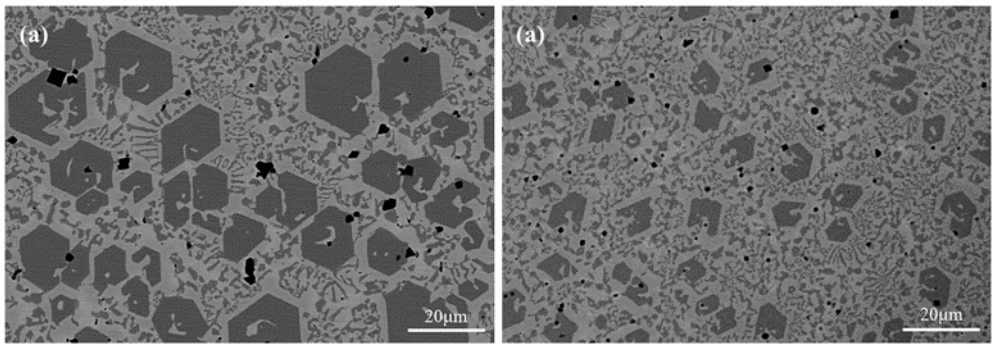

Fig. 8. Back-scattering micrographs of (a) hy- pereutectic Fe-Cr-C-Ti coating and (b) hyper- eutectic Fe-Cr-C-Ti- Y_2O_3 coating.